Geometric Constant Defining Shape Transitions of Carbon Nanotubes under Pressure

Ji Zang,[1] Andrejs Treibergs,[2] Y. Han,[1] and Feng Liu[1,*]

[1]*Department of Materials Science and Engineering, University of Utah, Salt Lake City, Utah 84112, USA*
[2]*Department of Mathematics, University of Utah, Salt Lake City, Utah 84112, USA*

(Received 12 August 2003; published 10 March 2004)

We demonstrate that when a single-walled carbon nanotube is under pressure it undergoes a series of shape transitions, first transforming from a circle to an oval and then from an oval to a peanut. Most remarkably, the ratio of the area of the tube cross sections at the second transition over that at the first transition appears as a constant, independent of the tube radius. Its accurate value is computed to be $G = 0.819\,469$, by formulating a variational geometry problem to represent single-walled carbon nanotubes with a family of closed plane curves of fixed length and minimum bending energy. The implications of such a geometric constant in designing nanotube electromechanical pressure sensors are discussed.

DOI: 10.1103/PhysRevLett.92.105501 PACS numbers: 81.07.De, 73.63.Fg, 85.35.Kt

The discovery of geometric relations and the calculation of geometric constants are among the very first scientific activities by human beings striving to understand nature. One well-known geometric constant is π, the ratio of a circle's circumference to its diameter. Its discovery and calculation, going back thousands of years [1], greatly stimulated the development of mathematics as well as science in general. Geometry is also one of the most fascinating and intriguing properties possessed by carbon nanotubes [2]. The electronic properties of a carbon nanotube are intrinsically linked with its geometry, in particular, its radius and chirality.

Here, we demonstrate the existence of a geometric constant that defines the shape transitions of single-walled carbon nanotubes (SWNTs) under hydrostatic pressure. Computer simulations show that, when a SWNT deforms under pressure, it undergoes two shape transitions: first changing from a circle to an oval and then from an oval to a peanut. Most surprisingly, the ratio of the cross-sectional areas at these two transitions is found to be a constant, the same for all SWNTs. The pressure-induced shape transitions of SWNTs can be understood in terms of the classical theory of elastic rings. We formulate a variational geometric problem, which confirms the existence of a geometric constant that defines a closed plane curve of fixed length changing from a convex (circle and oval) to a nonconvex (peanut) shape maintaining the minimum bending energy. The mathematical formulation allows us to compute the accurate value of this geometric constant to be 0.819 469.

Recently, there have been extensive studies of the structural and mechanical properties of carbon nanotubes under pressure [3–11]. We have performed computational experiments to investigate the correlation between mechanical and electrical properties in SWNTs under hydrostatic pressure, in an attempt to design nanoscale tunable pressure sensors [12]. We have simulated the equilibrium shapes of armchair and zigzag tubes under pressure, using a constant-pressure molecular dynamics (MD) method [13]. Figure 1 shows the evolution of tube cross sections with increasing pressure for (6,6), (12,12), and (18,18) armchair tubes. (Similar results are obtained for zigzag tubes.) The pressure induces mechanically two shape transitions: first transforming the tube cross section from a circle to an oval shape (dark, purple online) and then from an oval (convex) to a peanut (nonconvex) shape (dark, red online).

The first shape transition from circle to oval can be understood by the continuum theory of the buckling of

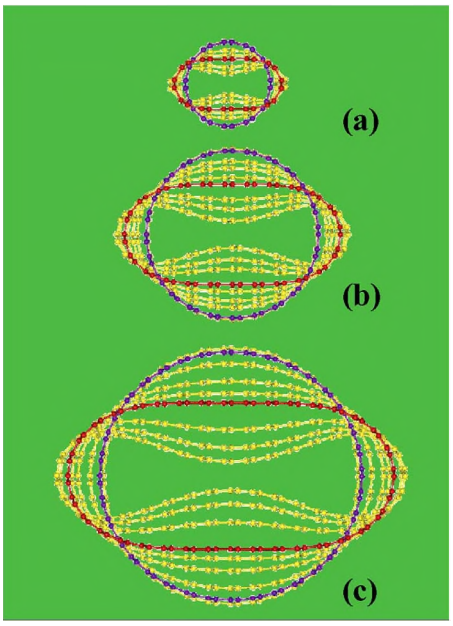

FIG. 1 (color online). Evolution of cross sections of armchair SWNTs under hydrostatic pressure, obtained from MD simulations. (a) (6,6), (b) (12,12), (c) (18,18) tube. The dark circle tubes (purple online) mark the first transition from circle to oval and the dark oval tubes (red online) mark the second transition from oval to peanut. For all the tubes, the ratio of cross-sectional area of the dark oval tube (red online) to the dark circle tube (purple online) is found to be constant.

elastic rings [14–16]. The transition pressure depends on the tube radius R as $P_1 = (3D)/R^3$ [14], where D is the flexural rigidity of the tube. Our MD simulations confirm that this relation does indeed describe the behavior of SWNTs. This implies that continuum mechanics is even applicable down to the smallest tube we simulated, whose cross section contains only ~10 atoms. It is interesting to note that the classical buckling theory of elastic rings was originally considered primarily for academic interest [14–16], yet it has found new significance in the nanoworld, with potential technological implications.

Physically, the first transition is driven by competition between compression and bending of a tube under pressure. As a circular tube shrinks by reducing its radius, it costs both compressive strain energy, due to reduced perimeter, and bending strain energy, due to increased curvature. Because it is easier to bend than to compress a tube, the tube transforms spontaneously from an isotropic circle to an anisotropic oval shape at a critical pressure P_1, and thereafter it no longer compresses (maintaining its perimeter) but only bends (reducing its overall curvature). Microscopically, this corresponds to the fact that it costs less energy to change the bond angle than to change the bond length.

As the tube continues to shrink, reducing its cross-sectional area after the first transition, it must adopt a shape that minimizes bending energy. This eventually leads to the second shape transition from a convex oval to a nonconvex peanut shape at a pressure P_2. Most surprising and interesting, this second transition is found to occur always at a point defined by a universal constant in relation to the first transition, independent of the original tube radius.

In Fig. 2, we plot the ratio of the tube cross-sectional area (A_2/A_1) at the second transition point (P_2) to that at the first point (P_1). It appears to be the same (~0.82) for

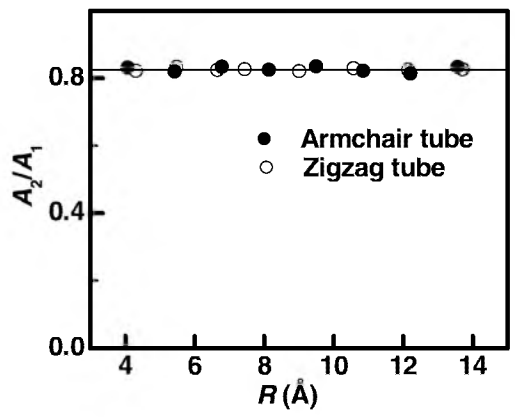

FIG. 2. The simulated ratio of tube cross-sectional area at the second transition [dark oval tube (red online) of Fig. 1] to that at the first transition [dark circle tube (purple online)]. It appears to be constant ~0.82, as indicated by the horizontal line. The small variations of data are due to uncertainty in determining the exact shape transition points in the simulation.

all the tubes we simulated, ranging from (6,6) to (28,28) for armchair and (10,0) to (35,0) for zigzag tubes. Figure 2 shows the results for tubes with radii from 4 to 14 Å. This indicates the existence of a geometric constant, as the second transition is a purely geometric transition without changing the tube's physical properties. Mechanically, the first transition changes the tube from both compression and bending to pure bending, while the second transition changes only the tube geometry from a convex to a nonconvex shape, but the tube still deforms by pure bending. Below we formulate a variational geometry problem using a family of closed plane curves to represent the SWNT shapes from the first to the second transition, which confirms the existence of such a geometric constant and facilitates numerical computation of its accurate value.

Consider smooth embedded closed curves in the plane $\Gamma \subset \boldsymbol{R}^2$, which bound a compact region Ω having a given boundary length L_0 and enclosing an area A. Among such curves we seek one, Γ_0, which minimizes the bending energy, $E(\Gamma) = \int_\Gamma \mathrm{K}^2\, ds$, where K is the curvature. We are interested in the relation between the geometry of the minimizer and the values of varying A.

We first realize that the problem is invariant under a homothetic scaling of Γ_0. If the curve is scaled to $\Gamma_0 = c\Gamma_0$, its area, length, and energy change by $A_0 = c^2 A_0$, $L_0 = cL_0$, and $E = c^{-1}E$ for $c > 0$. Consequently, the shape of the minimizer, and, hence, any dimensionless measure of the shape is a constant, independent of the scaling. Thus, we confirm that, if SWNTs can be represented by such a family of closed plane curves, there must exist a geometric constant that defines the SWNT shape transitions by the dimensionless measure of the ratio of area, A_2/A_1, with A_1 and A_2 being the areas at the transition points.

The isoperimetric inequality says that the area of any figure with a fixed boundary length does not exceed the area of a circle; hence, the ratio of the area $\mathcal{G} = A_2/A_1$ satisfies $0 < \mathcal{G} \leq 1$, and $\mathcal{G} = 1$ only for the circle. Next, we describe a self-consistent procedure to compute numerically the value of $\mathcal{G}$ that defines the convex-to-nonconvex shape transition.

Let s denote arclength along the curve Γ_0. The position vector is $X(s) = (x(s), y(s))$ and the unit tangent vector is $T(s) = (x'(s), y'(s)) = (\cos\theta(s), \sin\theta(s))$, where $\theta(s)$ is the angle T makes with the x axis, as shown in Fig. 3. The prime denotes differentiation with respect to arclength. The position can then be recovered by integration as $X(s) = X_0 + \int_0^s (\cos\theta(t), \sin\theta(t))\, dt$. The curvature is $\mathrm{K} = \theta'(s)$.

Assuming that the curve of the minimizer has reflection symmetry in both the x and y directions, we only need to find θ for $0 < s < L_4$, with $4L_4 = L_0$, over a quarter of the curve (Fig. 3). It is necessary that $\theta(L_4) = \pi/2$ for the curve not to have corners at the reflection points. So the variational problem is to find a function θ: $[0, L_4] \to \boldsymbol{R}$ such that $\theta(0) = 0$ and $\theta(L_4) = \pi/2$

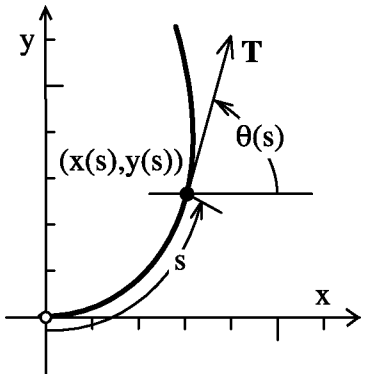

FIG. 3. Coordinates for one quadrant of the closed plane curve.

satisfying $\text{Area}(\theta) = A_4 = A/4$, which minimizes the bending energy $E(\Gamma)$. The corresponding Lagrange functional is

$$L_4[\gamma] = \int_\gamma \mathrm{K}(s)^2\, ds - \lambda\left\{A_4 - \int_\gamma x\, dy\right\} = \int_0^{L_4} \dot{\theta}(s)^2\, ds - \lambda\left\{A_4 - \int_0^{L_4}\int_0^s \cos\theta(t) dt \sin\theta(s)\, ds\right\}. \quad (1)$$

The variational minimization of $L_4[\gamma]$ leads to the following Euler Lagrange integrodifferential equation [17]

$$\ddot{\theta}(s) = -\frac{\lambda}{8}\left\{\sin\theta(s)\int_s^{L_4}\sin\theta(t)\, dt - \cos\theta(s)\int_0^s \cos\theta(t)\, dt\right\}. \quad (2)$$

Differentiating Eq. (2) gives the following curvature relation [17]:

$$(\mathrm{K}')^2 = c_1\mathrm{K}^2 + c_2 + \frac{\lambda\mathrm{K} - \mathrm{K}^4}{4} = F(K), \quad (3)$$

where c_1 and c_2 are integration constants.

The curvature must be an L_0-periodic function for a closed curve, which satisfies the nonlinear spring equation of Eq. (3). Because the curvature is continuous and has reflection symmetry at the end points, it must also be an even function at the end points, having $\mathrm{K}'(0) = \mathrm{K}'(L_4) = 0$. Thus, the noncircular periodic solution of K having the largest period of $L_0/2$ (i.e., the minimum bending energy) must adopt an oval or peanut shape, with the minimum and maximum curvatures at the endpoints of the quarter curve. Because the minimum K may be negative, as in the peanut shape, the embeddedness of the reflection is satisfied if $\mathrm{K}(0) = \mathrm{K}_1$ is the maximum and $\mathrm{K}(L_4) = \mathrm{K}_2$ is the minimum curvature around the curve, as shown in Fig. 3.

As K and K′ vary, the parameters c_1, c_2, and λ must allow solvability of Eq. (3). Moreover, $F(\mathrm{K}_1) = F(\mathrm{K}_2) = 0$, and given $\mathrm{K}_1 \neq -\mathrm{K}_2$ we have

$$c_1 = \frac{1}{4}\left(\mathrm{K}_1^2 + \mathrm{K}_2^2 - \frac{\lambda}{\mathrm{K}_1 + \mathrm{K}_2}\right), \quad (4)$$

$$c_2 = -\frac{\mathrm{K}_1\mathrm{K}_2}{4}\left(\mathrm{K}_1\mathrm{K}_2 - \frac{\lambda}{\mathrm{K}_1 + \mathrm{K}_2}\right). \quad (5)$$

Since the possible homotheties and translations of the same solution [shifts like $\mathrm{K}(s + c)$] have been eliminated, the remaining condition on the constants of integration is to ensure that the direction angle θ changes by exactly $\pi/2$ over γ, i.e.,

$$\theta(L_4) = \int_0^{L_4} \mathrm{K}(s)\, ds = \pi/2, \quad (6)$$

which can be reduced to complete elliptic integrals.

Thus, the variational problem can be solved by choosing a K_2 and determining K_1 self-consistently using Eqs. (4)–(6). Figure 4(a) shows a set of numerical solutions of curves with the largest period of $L_0/2$ ($n = 2$), as a function of ratio $\mathcal{G}$. Most remarkable, we found these curves match exactly, with a proper scaling, to those contours of the tube cross sections of Fig. 1. Therefore, the mathematical formulated shapes represent exactly the pressure-induced SWNTs' shape transitions.

In Table I, we tabulate the selected data of ratio ($\mathcal{G}$), the aspect ratio (X to Y), the maximum curvature (K_1), and the minimum curvature (K_2), for some shapes from the $n = 2$ solutions [Fig. 4(a)]. They are all single-valued

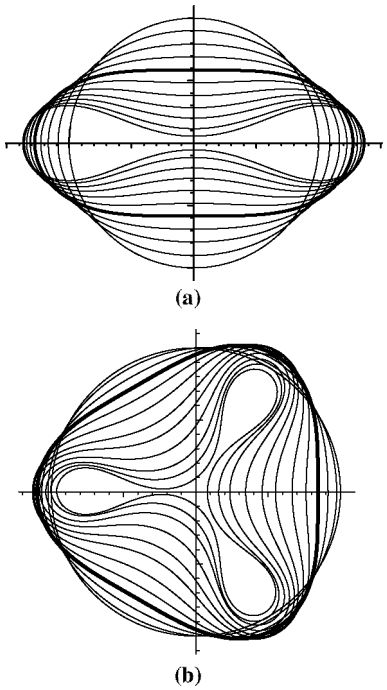

FIG. 4. (a) Numerical solutions of the variational geometric curves with period of $L_0/2$. The bold line marks the convex-to-nonconvex transition with the minimum curvature $K_2 = 0$. (b) Same as (a) with period of $L_0/3$.

TABLE I. Data of area ratio ($\mathcal{G}$), aspect ratio (X to Y), maximum curvature (K_1), and minimum curvature (K_2), for shapes from $n = 2$ solutions, as shown in Fig. 4(a). The bold line marks the data at the convex-to-nonconvex transition point ($K_2 = 0$).

$\mathcal{G}$	X to Y	K_1	K_2
1.0	1.0	0.346 681	0.346 681
0.969 301	0.747 252	0.500 311	0.2
0.911 147	0.598 089	0.615 898	0.1
0.819 469	**0.458 052**	**0.745 404**	**0**
0.688 845	0.319 027	0.759 399	−0.1
0.5069	0.168 724	0.773 624	−0.2

monotonic functions. The point of $K_2 = 0$ defines the transition from convex oval to nonconvex peanut shape, giving $\mathcal{G} = 0.819\,469$, the geometry constant we are searching for.

There are other possible solutions with K having a smaller period of L_0/n with $n \geq 3$. We note that we must have at least $n = 2$ (four critical points of curvature) because of the Four Vertex Theorem for closed plane curves [18]. Figure 4(b) shows solutions for $n = 3$. However, the calculated bending energies for this family of solutions (as well as other families with larger n) are higher than those for the $n = 2$ family.

It is rather remarkable that the discovery of a geometric constant, an ancient scientific endeavor, is brought out in the study of carbon nanotubes, a modern research topic. Conversely, such an "ancient-type" discovery has important implications in modern science and technology. One area of impact is the very place where it was discovered, as the constant is a critical parameter that defines quantitatively the shape transitions of nanotubes under pressure. For example, we have found [12] that the further increase of pressure beyond the second shape transition will induce an electrical transition in the tube: A metallic armchair tube becomes semiconducting. Such correlated mechanical and electrical transitions provide the basis for designing electromechanical pressure sensors. The pressure and the cross-sectional area at the transition points are related, by definition of modulus, as $P_1 - P_2 = M_b \ln(A_2/A_1) = M_b \ln\mathcal{G}$. Here M_b is the bending modulus, because only bending deformation occurs from P_1 to P_2. Moreover, the transition pressures scale with tube radius, as $P_1 \sim 1/R^3$ [14]. Thus, it is possible to sense a different range of pressures by using tubes of different radii [12]. The constant $\mathcal{G}$ provides then a key parameter in calibrating the pressure range of the sensor.

Several pressure experiments [3–9] have been done on bundles of nanotubes and some [5,9] indicated the flattening of tubes under pressure, in analogy to the first transition we predict here for the single tube. However, in a bundle of tubes, the intertube van der Waals interaction influences also the tube shape. Therefore, a future pressure experiment on a single tube is awaited to confirm our prediction.

In conclusion, we discover a universal geometric constant that defines quantitatively shape transitions of SWNTs under hydrostatic pressure, from both molecular simulations and variational geometry analysis. Although such a constant is discovered for carbon nanotubes, it should universally govern shape transitions of any type of tubes under pressure. Furthermore, we expect similar shape transitions to appear in three dimensions for closed surfaces, such as human red blood cells [19,20], fluid membranes [21], and container walls [22]. All these physical objects are believed to adopt shapes controlled by minimizing bending energy, the context within which the discovered geometry constant occurs universally.

This work is partly supported by DOE (DE-FG03-01ER45875; -03ER46027). Y. H. is supported by NSF (DMR0307000).

*Electronic address: fliu@eng.utah.edu

[1] P. Beckmann, *A History of π* (St. Martin's Press, New York, 1971).
[2] For a review of geometry of carbon nanotubes, see M. S. Dresselhaus, G. Dresselhaus, and R. Saito, Carbon **33**, 883 (1995).
[3] U. D. Venkateswaran *et al.*, Phys. Rev. B **59**, 10 928 (1999).
[4] J. Tang *et al.*, Phys. Rev. Lett. **85**, 1887 (2000); M. J. López *et al.*, *ibid.* **86**, 3056 (2001).
[5] M. J. Peters *et al.*, Phys. Rev. B **61**, 5939 (2000).
[6] S. M. Sharma *et al.*, Phys. Rev. B **63**, 205417 (2001).
[7] S. Rols, Phys. Rev. B **64**, 153401 (2001).
[8] S. Reich, C. Thomsen, and P. Ordejón, Phys. Rev. B **65**, 153407 (2002).
[9] J. Sandler *et al.*, Phys. Rev. B **67**, 035417 (2003).
[10] T. W. Tombler *et al.*, Nature (London) **405**, 769 (2000).
[11] J.-Q. Lu *et al.*, Phys. Rev. Lett. **90**, 156601 (2003).
[12] J. Wu, J. Zang, B. Larade, H. Guo, X. G. Gong, and Feng Liu (to be published).
[13] D. Y. Sun and X. G. Gong, J. Phys. Condens. Matter **14**, L487 (2002).
[14] M. Levy, J. Math. Ser. **3**, 7 (1884).
[15] G. F. Carrier, J. Math. Phys. **26**, 94 (1947).
[16] J. Chaskalovic, Z. Angew. Math. Phys. **46**, 149 (1995), and references therein.
[17] Here, we present only the main idea of solution process. The detailed mathematical derivation will be published elsewhere.
[18] M. Do Carmo, *Differential Geometry of Curves and Surfaces* (Prentice-Hall, Englewood Cliffs, NJ, 1976), p. 37.
[19] P. Canham, J. Theor. Biol. **26**, 61 (1970).
[20] H. Deuling and W. Helfisch, Biophys. J. **16**, 861 (1976).
[21] H. Deuling and W. Helfisch, J. Phys. (France) **37**, 1335 (1976).
[22] J. Opea, American Mathematical Society, Student Mathematical Library 10, Providence, 147 (2000).